Mutations in *GALNT3*, encoding a protein involved in O-linked glycosylation, cause familial tumoral calcinosis

Orit Topaz[1–3], Daniel L Shurman[4], Reuven Bergman[1–3], Margarita Indelman[1,2], Paulina Ratajczak[4], Mordechai Mizrachi[1–3], Ziad Khamaysi[1], Doron Behar[3], Dan Petronius[1], Vered Friedman[3], Israel Zelikovic[3,5], Sharon Raimer[6], Arieh Metzker[7], Gabriele Richard[4] & Eli Sprecher[1–3]

Familial tumoral calcinosis (FTC; OMIM 211900) is a severe autosomal recessive metabolic disorder that manifests with hyperphosphatemia and massive calcium deposits in the skin and subcutaneous tissues. Using linkage analysis, we mapped the gene underlying FTC to 2q24–q31. This region includes the gene *GALNT3*, which encodes a glycosyltransferase responsible for initiating mucin-type O-glycosylation. Sequence analysis of *GALNT3* identified biallelic deleterious mutations in all individuals with FTC, suggesting that defective post-translational modification underlies the disease.

We assessed 12 individuals with FTC from two large kindreds of Druze and African-American origin (**Fig. 1a**) that have been extensively described[1,2]. All affected individuals reported recurrent painful, calcified subcutaneous masses of up to 1 kg (**Fig. 1b**), often resulting in secondary infection and incapacitating mutilation. Three individuals developed deep periarticular tumors (**Fig. 1b**), and one succumbed to the disease. All affected individuals had hyperphosphatemia (family 1, 6.2–8.5 mg dl^{-1}; family 2, 5.2–6.6 mg dl^{-1}) but normal levels of calcium, parathyroid hormone (PTH) and 1,25-dihydroxyvitamin D3.

With informed consent of all participants, we obtained DNA samples and carried out a genome-wide scan using 362 microsatellite markers (Research Genetics) in family 1. Consanguinity in this kindred allowed us to apply homozygosity mapping to identify in all affected individuals a 15-Mb segment identical by descent, flanked by *D2S142* and *D2S2284*/*D2S2177* on 2q24–q31 (**Fig. 1**). We obtained a maximum multipoint lod score of 6.7 (HOMOZ[3]). Multipoint linkage analysis in family 2 using seven markers in this critical region further reduced the interval to 3 Mb flanked by *D2S111* and *D2S1776* (**Fig. 1**) and yielded a maximum multipoint lod score of 3.4 (GeneHunter[4]).

Using Mapviewer, we identified 11 genes in the 3-Mb region associated with FTC. Of these, *B3GALT1*, *SCN7A*, *SCN9A*, *SCN1A* and *STK39* have roles in neural or neuroendocrine tissues; the functions of *TAIP-2*, *CMYA3*, *FLJ11457*, *LOC90643* and *LASS6* are mostly unknown. The last positional candidate gene, *GALNT3*, encodes the UDP-N-acetyl-alpha-D-galactosamine:polypeptide N-acetylgalactosaminyltransferase 3 (ppGaNTase-T3; ref. 5). ppGaNTase-T3 belongs to a large family of Golgi-associated biosynthetic enzymes that transfer GalNac from the sugar donor UDP-GalNac to serine and threonine residues and are thereby responsible for initiating O-glycan synthesis, a prevalent form of post-translational modification[6]. RT-PCR analysis showed strong expression of *GALNT3* in the skin and kidneys, two tissues of functional relevance to the pathogenesis of FTC[1,2] (**Fig. 2a**). Using balanced primer pairs, we screened PCR amplicons of all ten coding exons and conserved splice sites of *GALNT3* for pathogenic mutations in the genomic DNA of affected individuals (primer pairs and PCR conditions are available on request). Members of the Druze family carried a homozygous G→A transition at position 1524+1 (from the ATG translation start site), resulting in disruption of the intron 7 donor splice site consensus sequence (**Fig. 2b**). Affected individuals of family 2 were compound heterozygous with respect to a nonsense mutation 484C→T (starting from the ATG; resulting in the amino acid substitution R162X) in exon 1 and a splice site mutation (1524+5G→A) in intron 7 (**Fig. 2b**). PCR-RFLP analysis confirmed complete cosegregation of the mutations with the disease phenotype (**Fig. 2c**). All three mutations were not present in a panel of at least 290 chromosomes derived from healthy unrelated individuals.

Nonsense mutation 484C→T is expected to result in a nonfunctional null allele causing premature termination of protein translation. Mutations 1524+1G→A and 1524+5G→A alter the same splice donor site in intron 7. In contrast to the normal splicing score of 0.93 obtained for the intron 7 splice donor site predicted by the Splice Site Prediction by Neural Network software, the calculated score of this sequence carrying a G→A mutation at position 1524+1 or 1524+5 was 0.00. To further assess the consequences of the 1524+1G→A splice site mutation, we analyzed *GALNT3* gene transcription by RT-PCR, using RNA extracted from skin biopsy and blood samples from affected individuals in family 1. We detected no wild-type transcript and small amounts of an aberrant splice variant lacking the exon 7 nucleotide sequence (**Fig. 2d**). Exon 7 skipping leads to an in-frame deletion of 44 amino acid residues, destroying most of the linker region located between the catalytic domain and the ricin-like domain of the glycosyltransferase.

[1]Department of Dermatology, Rambam Medical Center; [2]Laboratory of Molecular Dermatology, Rambam Medical Center; and [3]The Bruce Rappaport Faculty of Medicine, Technion-Israel Institute of Technology, Haifa, Israel. [4]Department of Dermatology and Cutaneous Biology, Thomas Jefferson University, Philadelphia, Pennsylvania, USA. [5]Pediatric Nephrology Unit and Laboratory of Developmental Nephrology, Rambam Medical Center, Haifa, Israel. [6]Department of Dermatology, University of Texas Medical Branch, Galveston, Texas, USA. [7]Department of Dermatology, Tel Aviv-Sourasky Medical Center, Tel Aviv, Israel. Correspondence should be addressed to E.S. (e_sprecher@rambam.health.gov.il).

Published online 9 May 2004; doi:10.1038/ng1358

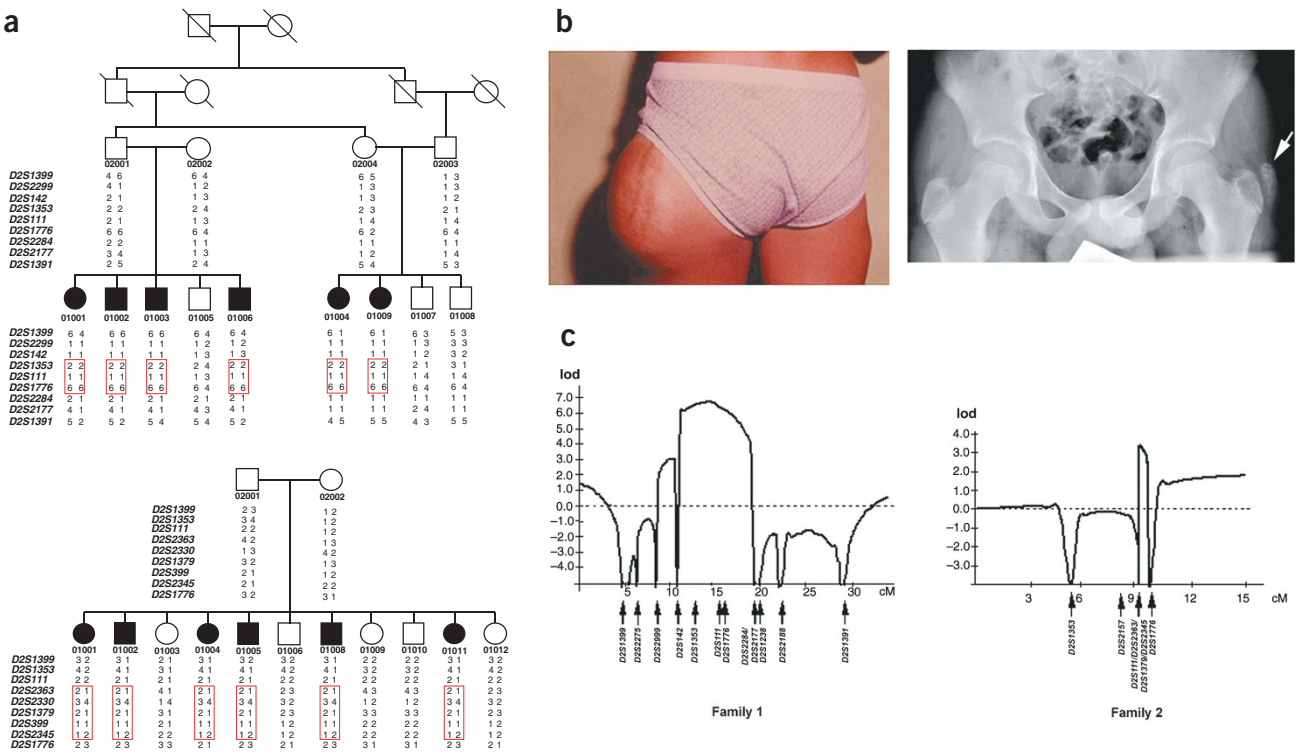

Figure 1 FTC mapping. (**a**) Haplotype analysis in two families with FTC using polymorphic microsatellite markers on 2q24–q31.1. The shared disease-associated haplotypes of all participating individuals are indicated by boxes. (**b**) Clinical features in FTC. The left panel shows a large subcutaneous tumor over the left outer thigh of individual 01001 of family 1. The right panel shows a periarticular calcified mass over the left acetabulum of individual 01006 of family 1. (**c**) Homozygosity mapping in family 1 (left panel) for 12 informative markers spanning 18.1 cM showed a maximum multipoint lod score of 6.7 at *D2S111* (using HOMOZ). The multipoint linkage map in the nonconsanguineous family 2 (right panel) using seven microsatellite markers shows a peak lod score of 3.4 for markers *D2S2363* and *D2S1379* (using GeneHunter).

Since the original description of FTC more than a century ago by Giard, the pathogenesis of this disease has been the subject of many investigations but has remained mostly elusive. Hyperphosphatemia, secondary to increased renal phosphate retention, is the major metabolic abnormality associated with FTC and is accompanied by inappropriately normal or elevated levels of PTH and 1,25-dihydroxyvitamin D3, two essential regulators of phosphate metabolism[7]. Additional molecules, such as fibroblast growth factor 23 (FGF23), secreted frizzled-related protein 4 (SFRP4) and matrix extracellular phosphoglycoprotein (MEPE), may also have roles in controlling circulating phosphate levels[7,8]. Those proteins have characteristics predicted for a new class of phosphate-regulating proteins collectively called phosphatonins[8] because they modulate circulating phosphate levels[9–12]. FTC seems to represent the metabolic mirror image of hypophosphatemic rickets caused by mutations in *PHEX* (OMIM 307800) and in *FGF23* (OMIM 193100)[7,8], which is characterized by decreased phosphate levels, decreased renal tubular phosphate reabsorption and inappropriately normal or decreased levels of 1,25-dihydroxyvitamin D3 (ref. 13). Hence, FGF23 and other phosphatonin genes have been considered prime candidates for underlying FTC[13].

Our results suggest a role for ppGaNTase-T3-mediated glycosylation in controlling phosphatonin activity. Although the NetOGlyc 3.0 software identified potential O-glycosylation sites in FGF23 (setting O-glycosylation score significance at >0.5), this molecule probably does not mediate the deleterious effects of *GALNT3* mutations in FTC. Impaired FGF23 activity in a mouse model led to prominent bone tissue abnormalities[14], which were absent in the individuals with FTC whom we studied. FGF23 circulating levels measured by ELISA (Immutopics) were significantly elevated in six individuals with FTC (1710 ± 864 RU ml^{-1}) as compared with six unaffected controls (56 ± 38 RU ml^{-1}), possibly reflecting a compensatory response to hyperphosphatemia. Thus, ppGaNTase-T3 may affect phosphate homeostasis by modulating the activity of another phosphatonin or PHEX[13]. Alternatively, it may directly regulate noncirculating elements in tissues where *GALNT3* is expressed (**Fig. 2a** and ref. 5), such as the skin (where calcium deposition occurs[1,2]), bone (where candidate phosphatonins are expressed[7,8]), kidneys and gastrointestinal tract (where phosphate transport occurs[13]). Given the existence of more than 20 ppGaNTase isoforms[6], substrate specificity or functional redundancy may account for the restricted nature of the FTC phenotype despite widespread *GALNT3* expression in tissues.

ppGaNTase-T3 may not be the sole regulator of phosphate homeostasis in peripheral tissues, as FTC can also present with normal blood phosphate levels[15]. Using haplotype analysis in four families with normophosphatemic FTC, we excluded linkage of this FTC variant to 2q24–q31 (data not shown), suggesting that normophosphatemic and hyperphosphatemic FTC are nonallelic disorders.

In summary, our results establish autosomal recessive mutations in *GALNT3* as the molecular cause of hyperphosphatemic FTC and demonstrate the pathological consequences of a genetic defect in a mucin-type O-glycosylation pathway. The identification of the gene underlying FTC should not only benefit the affected families, to whom molecular testing can now be offered, but may also shed new light on the mechanisms regulating phosphate metabolism in health

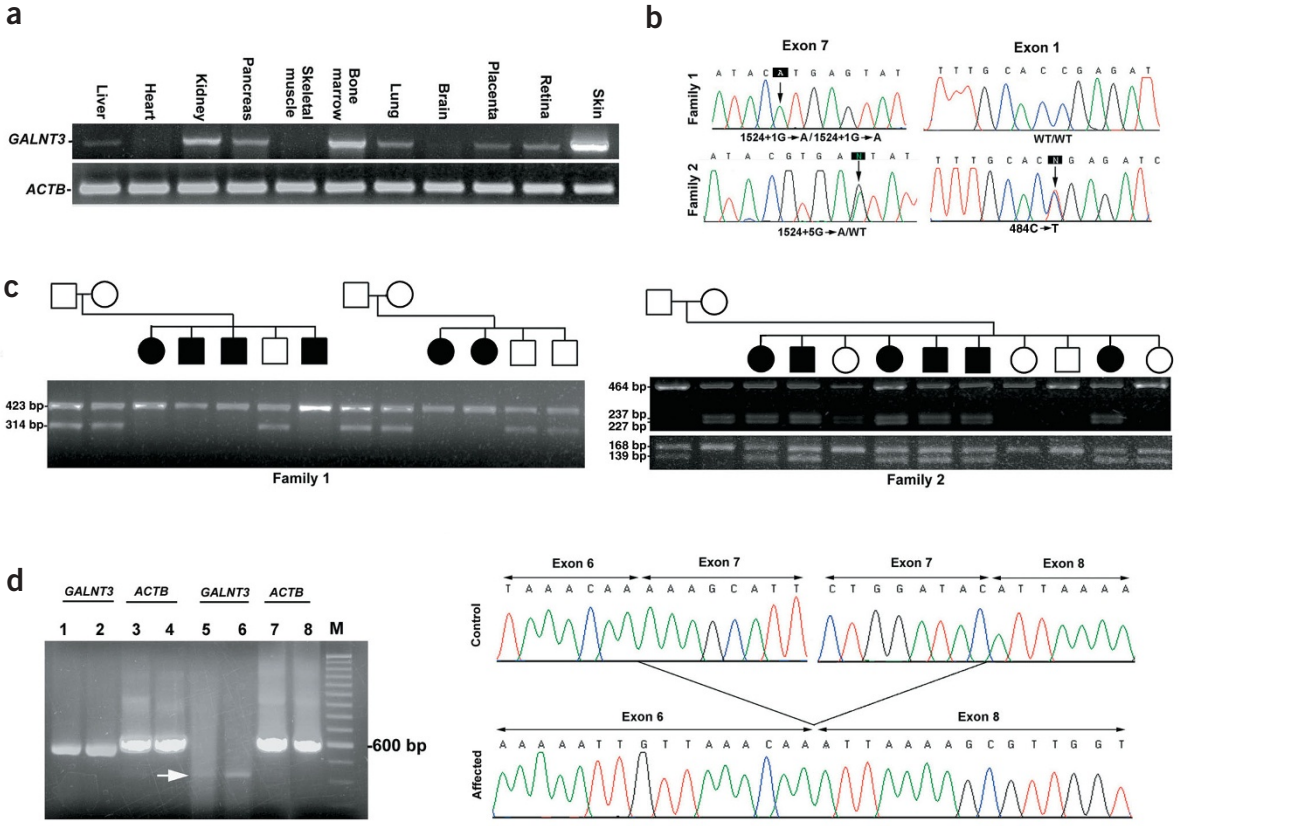

Figure 2 Gene expression and mutation analysis. (**a**) *GALNT3* gene expression was assessed using RT-PCR and primer pairs specific for *GALNT3* and *ACTB* in various tissues. (**b**) Sequence analysis showed a homozygous G→A transition at cDNA position 1524+1 in affected individuals of family 1 (left upper panel). In family 2, all affected individuals were compound heterozygous with respect to a G→A transition at cDNA position 1524+5 (left lower panel) and a C→T transition at cDNA position 484 (right lower panel). The wild-type sequence of exon 1 is shown in the right upper panel. (**c**) Segregation of the pathogenic mutations in families 1 and 2 is shown by restriction fragment analysis. 1524+1G→A abolishes a recognition site for *Bsa*AI; consequently, digestion of a PCR amplicon encompassing exon 7 generates a homozygous (uncut) 423-bp product in affected individuals of family 1, whereas heterozygous carriers of the mutation show a 314-bp fragment (an additional 109-bp fragment is not visible). In contrast, 1524+5G→A and 484C→T create new recognition sites for endonucleases *Ssp*I (upper gel) and *Dde*I (lower gel), respectively. Hence, affected individuals in family 2 have an additional fragment after digestion of the relevant PCR amplicons (exons 1 and 7) with the corresponding restriction enzymes. (**d**) Expression of *GALNT3* assessed by RT-PCR in the skin (lanes 1,3,5,7) and blood lymphocytes (lanes 2,4,6,8) of a healthy control (lanes 1,2,3,4) and of individual 01001 of family 1 (lanes 5,6,7,8; left panel). Note the low amounts and smaller size of the *GALNT3* RT-PCR product in the affected individual (arrow). *ACTB* RNA levels were comparable in the affected individual and the control. Sequencing of nested RT-PCR amplicons showed absence of exon 7 sequence in the aberrant splice product from the affected individual's skin and blood samples (right panel).

and disease, with obvious implications for the treatment of acquired disorders manifesting with hyperphosphatemic calcinosis, such as chronic renal failure.

URLs. Mapviewer is available at http://www.ncbi.nlm.nih.gov/mapview/. Splice Site Prediction by Neural Network is available at http://www.fruitfly.org/seq_tools/splice.html. NetOGlyc 3.0 is available at http://www.cbs.dtu.dk/services/NetOGlyc.

ACKNOWLEDGMENTS
We thank the families with FTC for participating in this study, H. Sprecher and I. Avidor for their help with the FGF23 ELISA assay and R. Fuhrer-Mor for DNA sequencing services. This study was supported in part by the Technion Research Fund (E.S.), the Chief Scientist Office- Israeli Ministry of Health (E.S. and R.B.) and grants from the US National Institutes of Health, National Institute of Arthritis and Musculoskeletal and Skin Diseases (G.R.).

COMPETING INTERESTS STATEMENT
The authors declare that they have no competing financial interests.

Received 1 March; accepted 16 April 2004
Published online at http://www.nature.com/naturegenetics/

1. Steinherz, R. *et al. Am. J. Dis. Child.* **139**, 816–819 (1985).
2. Slavin, R.E., Wen, J., Kumar, D. & Evans, E.B. *Am. J. Surg. Path.* **17**, 788–802 (1993).
3. Kruglyak, L., Daly, M.J. & Lander, E.S. *Am. J. Hum. Genet.* **56**, 519–527 (1995).
4. Kruglyak, L., Daly, M.J., Reeve-Daly, M.P. & Lander, E.S. *Am. J. Hum. Genet.* **58**, 1347–1363 (1996).
5. Bennett, E.P., Hassan, H. & Clausen, H. *J. Biol. Chem.* **271**, 17006–17012 (1996).
6. Ten Hagen, K.G., Fritz, T.A. & Tabak, L.A. *Glycobiology* **13**, 1R–16R (2003).
7. Schiavi, S.C. & Kumar, R. *Kidney Int.* **65**, 1–14 (2004).
8. Quarles, L.D. *Am. J. Physiol. Endocrinol. Metab.* **285**, 1–9 (2003).
9. Shimada, T. *et al. Proc. Natl. Acad. Sci. USA* **98**, 6500–6505 (2001).
10. Bowe, A.E. *et al. Biochem. Biophys. Res. Comm.* **284**, 977–981 (2001).
11. Rowe, P.S.N. *et al. Bone* **34**, 303–319 (2003).
12. Berndt, T. *et al. J. Clin. Invest.* **112**, 785–794 (2003).
13. Jan De Beur, S.M. & Levine, M.A. *J. Clin. Endocrinol. Metab.* **87**, 2467–2473 (2002).
14. Shimada, T *et al. J. Clin. Invest.* **113**, 561–568 (2004).
15. Prince, M.J. *et al. Ann. Intern. Med.* **96**, 586–591 (1982).